Intelligent cable shovel excavation modeling and simulation

Frimpong, S.; Hu, Y.

Publisher's version / Version de l'éditeur:
https://doi.org/10.1061/(ASCE)1532-3641(2008)8:1(2)
International Journal of Geomechanics, 8, 1, pp. 2-10, 2009-01-01

Intelligent cable shoved excavation modeling and simulation

NRCC-51124

Frimpong, S.; Hu, Y.

2008-01-01

A version of this document is published in / Une version de ce document se trouve dans:
International Journal of Geomechanics, v. 8, no. 1, pp. 1-10,
DOI: http://dx.doi.org/10.1061/(ASCE)1532-3641(2008)8:1(2)

Intelligent Cable Shovel Excavation Modeling and Simulation

Samuel Frimpong[1] and Yafei Hu[2]

Abstract: Cable shovel excavators are used for primary production of geomaterials in many surface mining operations. A major problem in excavation is the variability of material diggability, resulting in varying mechanical energy input and stress loading of shovel dipper-and-tooth assembly across the working bench. This variability impacts the shovel dipper and tooth assembly in hard formations. In addition, the geometrical constraints within the working environment impose production limitations resulting in low production efficiency and high operating costs. An intelligent shovel excavation (ISE) technology has been proposed as a potential solution to these problems. This paper addresses the requirements of the dynamic models of the cable shovel underlying the ISE technology. The dynamic equations are developed using the Newton–Euler techniques. These models are validated with real-world data and simulated in a virtual prototype environment. The results provide the path trajectories, dynamic velocity and acceleration profiles, and dimensioned parameters for optimum feed force, torques and momentum of shovel boom-dipper assembly for efficient excavation. The optimum digging forces and resistances for the cable shovel excavators are modeled and used to predict optimum excavation performance.

DOI: 10.1061/(ASCE)1532-3641(2008)8:1(2)

CE Database subject headings: Excavation; Mining; Simulation; Artificial intelligence.

Introduction

Shovel excavators are widely used as primary production equipment in surface mining operations for removing overburden and ore materials. The shovel–truck mining method in surface mining is flexible, efficient, and it can be easily relocated to different operating environments. The efficiency and costs of mining operations greatly depend on the efficient use of these capital-intensive shovel excavators. However, the shovel–truck mining method can be rendered inefficient from operating, environmental, topography, and operator constraints. Any naturally occurring formation is characterized by the defining properties of the constituent soils and rocks. These properties are shaped by the pre- and postformation chemical and mechanical processes to yield the relative ease of digging or excavating the formation. Thus, an excavator's cutting force is a function of the formation properties, machine–formation interactions and the operating parameters of an excavator. The formation parameters include cohesion, internal friction angle, density, water saturation, formation hardness and compaction, abrasiveness, the angle of formation failure wedge, and shear plane angle. The machine–formation interaction parameters include adhesion and external friction angle. The operating parameters also include blade travel velocity, cutting angle, tool working depth beneath surface, and surcharge pressure acting vertically on formation surface. These defining characteristics must be controlled through optimization to yield efficient excavation.

Careful planning and execution of shovel operations, relocations, and interactions with other production equipment are therefore vital to efficient operating performance. In addition, the physical and mechanical properties of materials being excavated have severe impact on the efficiency of a shovel excavator. They usually result in varying mechanical energy input and stress loading of shovel dipper-and-tooth assembly across the working bench when the shovel dipper is in contact with mining surfaces during excavation. Stress development and fatigue failure in equipment components such as booms cause unplanned downtimes, reduced efficiency, and high production costs. Complex and unstructured mining environments have a huge impact on shovel dipper and tooth assembly. Often, space limitations may limit the shovel–truck mining process to a single backup method, which is highly inefficient and unproductive (Frimpong et al. 2003).

A potential solution to the problems described above is the application of an intelligent shovel excavation (ISE) system that is responsive to shovel–formation interactive forces with space geometry scanning capability during excavation as illustrated in Fig. 1 (Frimpong et al. 2001). Fig. 1 consists of a shovel excavator, vision systems, sensors, and receivers that work together to capture mechanical energy, stress, and resistance information from a mining face, with space geometry scanning capability, in real time. These data are transmitted, processed, and displayed on an on-board screen in the operator's cabin. An operator can therefore assess local variation in the bench environment based on the information displayed on the screen and make real-time decisions. These decisions may lead to fragmentation of extremely hard formations, in-pit blending and stockpiling of materials as per the plant requirements. This vision system may also be used to plan the three-dimensional (3D) space geometry requirements of the shovel–truck mining method. The results may also be used to develop virtual prototype simulators for training operators within safety and cost constraints (Frimpong and Hu 2004; Frimpong et al. 2003).

[1]Robert H. Quenon Endowed Chair and Professor of Mining Engineering, Univ. of Missouri-Rolla, Rolla, MO 65409. E-mail: frimpong@umr.edu

[2]Research Officer, National Research Council of Canada, Regina, SK, Canada

Note. Discussion open until July 1, 2008. Separate discussions must be submitted for individual papers. To extend the closing date by one month, a written request must be filed with the ASCE Managing Editor. The manuscript for this paper was submitted for review and possible publication on April 27, 2006; approved on August 1, 2006. This paper is part of the ***International Journal of Geomechanics***, Vol. 8, No. 1, February 1, 2008. ©ASCE, ISSN 1532-3641/2008/1-2–10/$25.00.

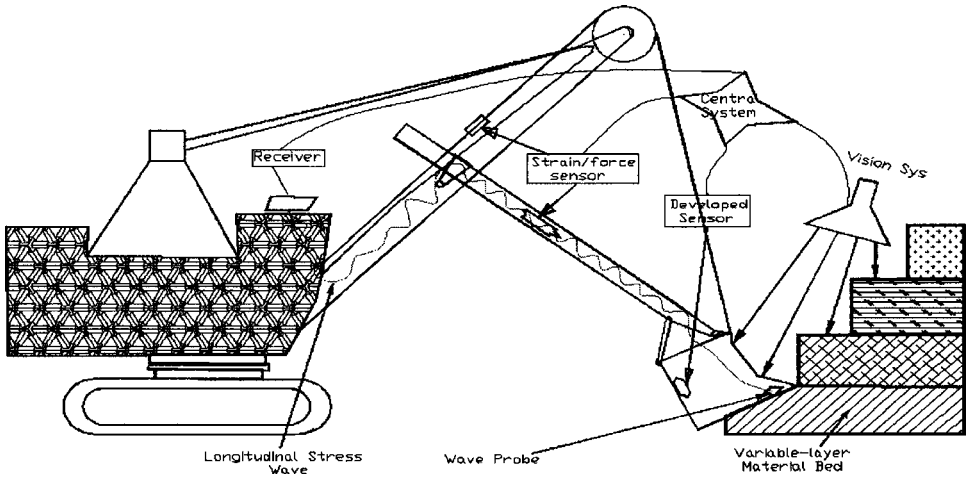

Fig. 1. Sensor-vision system in the ISE technology

The development of the ISE system requires kinematics and dynamic models of the shovel operating modes to describe the evolution of the excavator motion with time. Hendricks et al. (1993) developed a dynamic model for cable shovels using Lagrange formulations without including the resistive forces from the mined environments. Daneshmend et al. (1993) dealt with the same problem using an iterative Newton–Euler formulation. That work did not include the crowd arm and predictor models, which are very important for the complete description of the dynamic behavior of a cable shovel. In this paper, the dynamic models of shovel excavators are derived using the Newton–Euler formulation. These models are based on the main functional components of the cable shovel (the crowd arm and the dipper) as free bodies. The responses from the given digging trajectory are predicted. These models form the basis for developing comprehensive simulator models for efficient shovel operations in constrained mining environments and the development of the ISE technology for real-time excavation in surface mining operations.

Machine optimization provides the optimum feed force required to excavate a unit volume of material within an optimized trajectory for a given geological formation, with its geomechanical characteristics. This optimum feed force, within an optimized trajectory, is governed by a set of optimized machine parameters, which results in the least breakout force or energy during excavation. Cable shovel uses electrical energy for machine propel, crowding, hoisting, swinging, and excavation. Inefficient shovel excavation results in faster machine wear and tear, fatigue failure with corresponding higher maintenance and energy costs. The optimized parameters include crowd, hoist and swing speeds, and the configuration of the optimized trajectory. Awuah-Offei (2005) showed that shovel optimization could result in significant reductions in shovel digging time, digging energy per cycle and energy costs, with a corresponding increase in shovel production and productivity. The second section deals with a description of the cable shovel structural components. The following section deals with the development of the kinematics and dynamic models, the details of which are presented in the Appendix. The next section deals with numerical validation of a cable shovel dynamics. Then the work is concluded with the references and an Appendix. A notation section is included to provide definitions for all the variables and symbols used for the dynamic equations in this paper.

Cable Shovel Structural Components

The cable shovel is designed specifically to excavate and load materials in surface mining operations. This shovel has large breakout forces, lower maintenance, and production costs and higher economic useful life. The excavator's high availability and utilization factors results in efficient production operations. Fig. 2 illustrates the structural components of this shovel. It uses electric motors, gear reducers, drums and wire ropes to actuate the motions required for digging, loading and propelling. The capacity of these machines is typically 25 m^3 (33 yd^3) to 63 m^3 (82 yd^3) for standard rock applications. The cable shovel consists of three major assemblies: The lower frame, upper frame, and the attachment. The lower frame provides a stable base for the machine and includes the propel-drive and crawler system. The upper frame provides a platform for the hoist and swing machinery, and for boom attachment, electronic control cabinets, operator's cab, and supporting equipment. The attachment consists of the boom, crowd machinery, dipper handle, and dipper. The dynamics of this shovel includes propel, crowding, and retraction (reverse crowding), digging, loaded and empty swinging and dumping. These dynamic processes must be coordinated to ensure efficient operating performance within a constrained environment (P&H Mining 2003).

Dynamic Modeling of Cable Shovel Excavator

The cable shovel dynamic function comprises three major components, including inertia matrix, Coriolis and centripetal force effects and gravity effects. This dynamic function must be equivalent to the difference between the breakout force (from equipment) and the resistive force due to formation. Thus, the dynamic equation for the cable shovel excavators is given by

$$D(\Theta)\ddot{\Theta} + C(\Theta,\dot{\Theta})\dot{\Theta} + G(\Theta) = F - F_{\text{load}}(F_t, F_n) \tag{1}$$

The digging path of the dipper is produced by the extension/retraction of the handle (crowd) and by the cable hoisting action as in Figs. 2 and 3. Dipper hoisting is accomplished by means of cables attached to the dipper, which pass over sheaves at the boom point and spool on a deck mounted powered drum. The

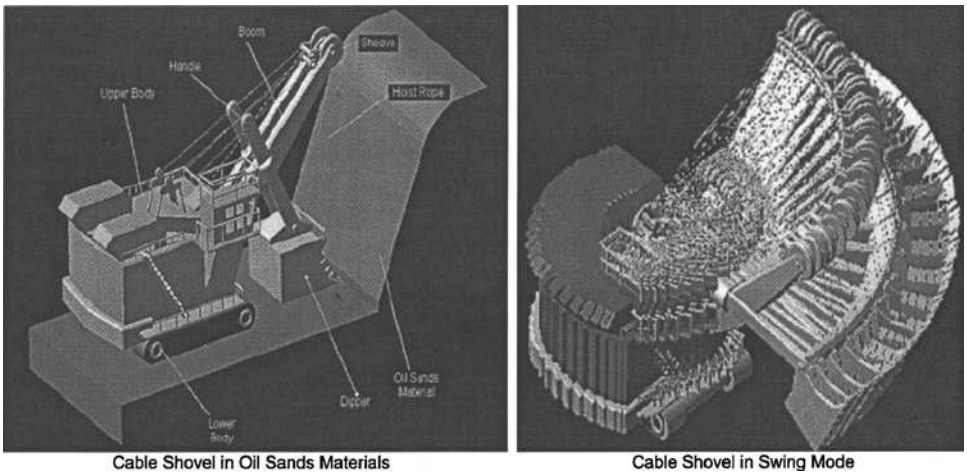

Fig. 2. Cable shovel nomenclature

crowd action is produced either by cables or a direct rack and pinion gear drive (P&H Mining 2003). In Fig. 3, $X_W Y_W Z_W$ =coordinates at the base and upper structures of the shovel, $O_0X_0Y_0Z_0$, $O_1X_1Y_1Z_1$, and $O_2X_2Y_2Z_2$=respective coordinates of the boom, crowd arm, and dipper. It is considered that the upper structures of the cable shovel are fixed, and thus, the kinematics and dynamic models of the shovel excavator are mainly related to crowd arm and dipper (Koiva 1994; Koivo et al. 1996; Vaha and Shibniewski 1993.

The dynamic equations can be obtained by applying either the Lagrange method or iterative Newton–Euler method. The iterative Newton–Euler method is used because the iterative formulation lends itself to efficient software implementation, which is of importance for real-time simulation and parameter estimation (Frimpong and Hu 2004; Frimpong et al. 2003; Daneshmend et al. 1993). Also, it provides detailed information on all links and joints, which is useful in stress and/or strength analysis of components. The Newton–Euler dynamic algorithm for computing the crowd force and the hoist torque comprises two parts. First, the velocities and accelerations are iteratively computed from the crowd arm to the dipper and the Newton–Euler equations are applied to each of them. Second, the interactive forces and torques and joint actuator torques are computed recursively from dipper back to crowd arm (Craig 1986). The detailed mathematical models for the cable shovel kinematics and dynamic models are outlined next in sections and in the Appendix.

Cable Shovel Kinematics

The shovel kinematics models are obtained for the front-end assembly, which comprises the boom, crowd arm, hoist rope, and dipper components as illustrated in Fig. 3. The angular and linear displacements, velocities and acceleration are established for the shovel base, boom, crowd arm, bucket, and the cutting edge of the dipper as illustrated in the Appendix. The Newton–Euler formulations are obtained for the outward and inner iterations as illustrated in the Appendix. The equations of the outward iterations govern the motion of the forward assembly when it is being extended to begin the excavation process. An empty dipper, higher angular and linear displacements and velocities and smaller moments about the centers of rotation characterize this motion. The equations of the inward iterations govern the motion of the forward assembly when it is being retracted after the excavation process. A loaded bucket, relatively slower angular and linear displacements and velocities and higher moments about the centers of rotation characterize this motion.

Cable Shovel Dynamics

The shovel dynamic models are obtained for the front-end assembly in Fig. 3. The dynamic models use the results of the kinematics as input to develop the models for inertial force, moments and resistive force. The active forces are used to generate the breakout forces required for the excavation process. The breakout force must exceed the resistive force for the formation to be removed from in situ. The resistive force is a resultant of the tangential and normal force incident on the plane of excavation as illustrated in Figs. 4 and 9. The resulting moments from the active forces and the centers of rotation about various joints are important in the overall shovel performance. The dynamic models are also developed for outward or backward and inner or inward iterations to examine the dynamics of the excavation process in the extension,

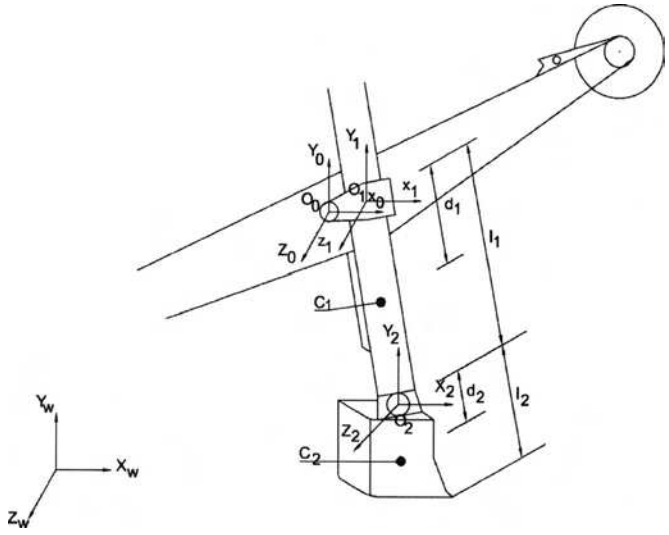

Fig. 3. Elements of shovel dynamics (adapted from Frimpong et al. 2003)

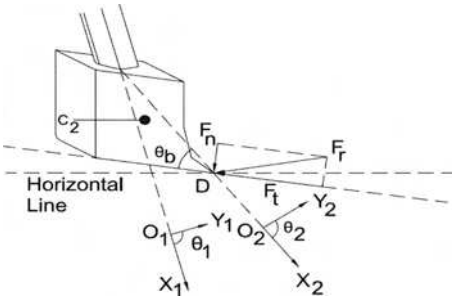

Fig. 4. Interaction between dipper and environment

excavation and retraction phases (Araya et al. 1998). The details of the dynamic models are presented in the appendix section.

Numerical Validation of Cable Shovel Dynamics

A scaled cable shovel model is used to validate the dynamic models in this study. The main geometry and physical data for the simulated shovel are listed in Table 1. The digging trajectory in Fig. 5 is first generated based on the physical and mechanical properties of the material being excavated using the reference coordinate system (X_W, Y_W, Z_W) in Fig. 3. Fig. 3 shows the trajectory for completing the digging section of a working cycle using this reference coordinate. The moments of inertia for the dipper and the dipper handle are considered at the mass center for each element. The length of the handle is the length between the end of the handle and the handle-dipper joint. The length of the dipper is the length between the handle-dipper joint and end of the dipper teeth. The following discussions are based on the results from detailed experimentation of the cable shovel simulator under various operating regimes.

Figs. 6–8 show the change of (d_1, θ_1), $(\dot{d}_1, \dot{\theta}_1)$, and $(\ddot{d}_1, \ddot{\theta}_1)$ with time t, respectively. The vertical axes, in Figs. 6–8, have been normalized for a comparative purpose. In Fig. 6, the linear displacement of the crowd arm, d_1, advances at first, experiences a maximum resistive force around the middle of the path profile and then retracts following the given digging profile, whereas the angular displacement of the crowd arm, θ_1, always increases with time. Although θ_1 is increasing constantly, its rate of change, $\dot{\theta}_1$, is not constant as illustrated in Fig. 7. It has a maximum around the path midpoint. For the crowd arm advance rate, $\dot{d}_1$, it is decreasing constantly as shown in Fig. 7. The crowd arm advance acceleration, $\ddot{d}_1$, and the angular acceleration, $\ddot{\theta}_1$, are more complex for the given digging path profile. The two accelerations increase and then decrease during the first half of the digging path and reverse for the latter half of the path. Figs. 6–8 also show that the crowd arm linear and rotational kinematics have different trends. It is important for planning engineers and operators to understand and control the machine kinematics to ensure efficient execution of the shovel trajectory within the limiting design and field constraints.

Table 1. Main Shovel Structural Data for Scaled Cable Shovel

Part	Length (m)	Mass (kg)	Inertia moments (kg m^2)
Handle	11.888	65,800	7.749E+5
Dipper	5.800	24,500	6.458E+4
Bucket capacity 30.6 m^3			

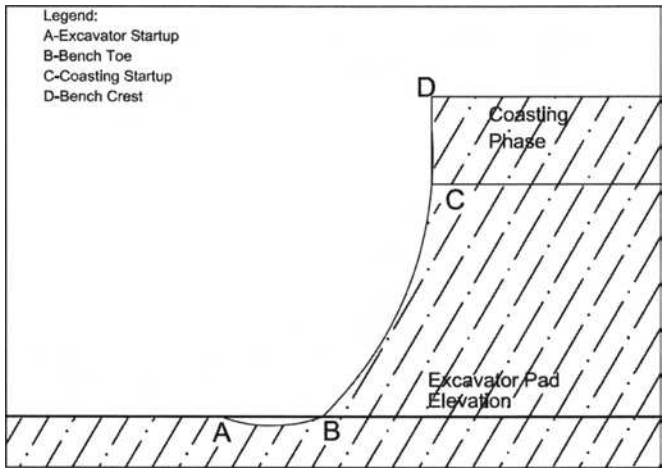

Fig. 5. A trajectory for a shovel dipper tip

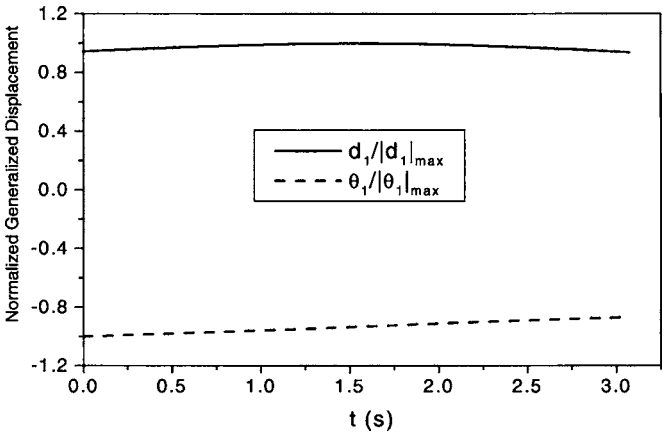

Fig. 6. Normalized linear (d_1) and angular (θ_1) displacements with time

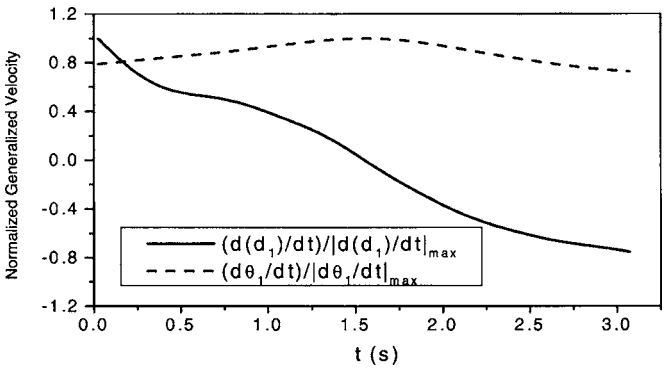

Fig. 7. Normalized linear $(\dot{d}_1)$ and angular $(\dot{\theta}_1)$ velocities with time

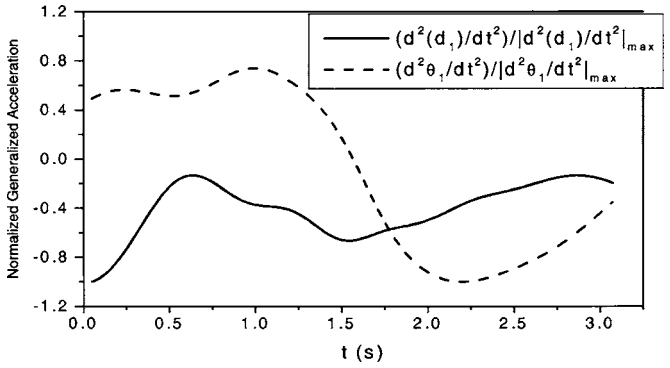

Fig. 8. Normalized linear ($\ddot{d}_1$) and angular ($\ddot{\theta}_1$) accelerations with time

The crowd arm for the given digging trajectory has a much smaller change than that of the arm rotation, indicating a predominant rotation effect in the inertial part. It is also noted that there are some erratic behaviors, especially in $\ddot{d}_1$ and $\ddot{\theta}_1$, which are attributed to the time differential of d_1 and θ_1. When d_1, $\dot{d}_1$, $\ddot{d}_1$, θ_1, $\dot{\theta}_1$, and $\ddot{\theta}_1$ are determined for each time, the normalized force and torque can be calculated, and their behavior with time is shown in Fig. 9. Fig. 9 shows that the crowding inertial force increases continuously and has a much bigger range. It indicates that the inertial force mainly comes from the rotation part. However, the torque requirements stay relatively constant, which indicates an efficient utilization of the breakout force requirements. Based on the Zelenin et al. (1985) model, the resistive force according to the current trajectory is calculated and shown in Fig. 10. Fig. 10 shows that the digging force is divided into three phases in a digging cycle: gradual increase, reaching a maximum and a gradual decrease to zero. Finally, F may be obtained from Eq. (1) as all other terms are already determined. Then the relationship between the crowd force and hoist torque from crowd and hoist motors and the resistance force F_r may be established. Thus, by measuring the crowd force and hoist torque, one can know the current resistance force from material diggability. Thus, from this analysis, the efficient breakout force, given certain diggability index, can be established and used for planning and executing different material excavation. This is a major contribution to large-scale costly excavation of material in surface mining operations.

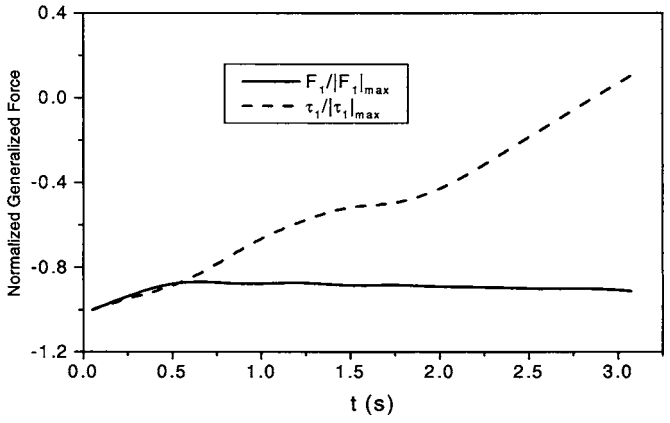

Fig. 9. Normalized inertial force and torque with time

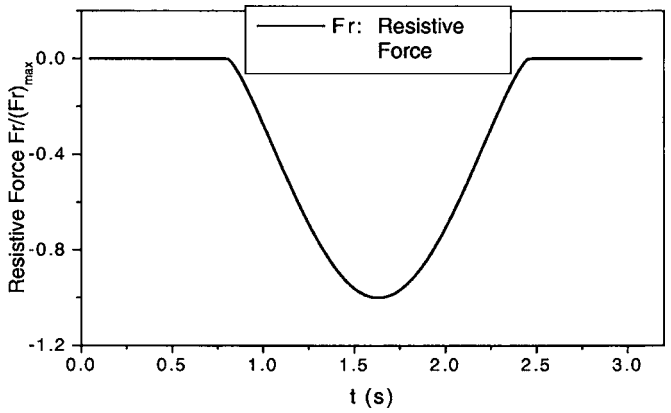

Fig. 10. Normalized resistive force with time

Optimum Shovel Performance. The results of the optimized machinery–formation interactions define the envelope for optimum digging performance. As illustrated by equations (24), (25), and (27), the formation resistant force depends on several variables that govern the geometry of machine–formation interactions. For efficient excavation in this paradigm, the results show that the normalized force, F_r, must be controlled based on Fig. 10. Given the maximum F_r based on the formation, the actual profile of the force required to overcome the formation resistance must increase from 0.25 to 1.63 s during the digging cycle and decrease with same gradient in a parabolic form as illustrated in Fig. 10. The normalized linear and angular displacement, velocity and acceleration and inertia force and torque profiles must also follow Figs. 6–9, respectively, for optimum excavation.

Conclusions

Dynamic models of cable shovel excavators have been derived for the main functional components (crowd arm and the dipper) as free body diagrams using an iterative Newton–Euler method. The responses from a given digging trajectory are predicted using a case study. The shovel kinematics results provide the optimum angular and linear displacements, velocities and acceleration for effective engagement of the formation by the dipper teeth. The dynamic models also yield the appropriate reactive forces, moments and torque, which are required for generating the required breakout forces given certain material diggability index for efficient excavation. Further research is required to characterize, model and simulate the interactions between the shovel and the mining environments. This will eventually enable complete simulation of the shovel operation, as well as, ore bench digging conditions assessment based on on-line data measurements from the main functional components of a shovel excavator. These results will form the basis for developing the intelligent shovel excavation technology.

Acknowledgments

The writers express their gratitude to the Robert H. Quenon Endowment, University of Missouri-Rolla, for financial support of this research.

Notation

The following symbols are used in this paper:

C_{ij} = (i,j) element of Coriolis and centripetal torque $C(\theta,\dot{\theta})\dot{\theta}$;
C_0 = compactness and cutting resistance index;
$C(\Theta,\dot{\Theta})$ = generalized Coriolis and centripetal torque;
c_1, s_1 = $\cos\theta_1$, $\sin\theta_1$ respectively;
$c_{\theta i}$, $s_{\theta i}$ = $\cos\theta_i$ and $\sin\theta_i$ (i,j), respectively;
$c_{\theta i\theta j}$, $s_{\theta i\theta j}$ = $\cos(\theta_1+\theta_j)$ and $\sin(\theta_i+\theta_j)(i,j)$, respectively;
D_{ij} = (i,j) element of inertia matrix $D(\theta)$;
$D(\Theta)$ = generalized inertia matrix;
d = cutting plate thickness;
d_i = offset distance of the gravity center in link i;
d_1, $\dot{d}_1$, $\ddot{d}_1$ = displacement, linear velocity and acceleration of crowd arm;
e_z = tool plate thickness;
F = cable shovel's breakout force;
$F_{\text{load}}(F_t,F_n)$ = resistive force due to the formation being excavated by the shovel dipper;
F_n = normal reaction force;
F_r = loading force acting on dipper from the soil;
F_r = resistive forces from formation material;
F_t = tangential reaction force;
${}^1F_1$ = inertial force at the center of the crowd arm;
${}^2F_2$ = inertial force at the center of the dipper;
f_{31}, f_{32} = respective x and y components of the interaction force between soil and dipper tip;
G_i = ith component of gravity torque $G(\theta)$;
$G(\Theta)$ = generalized gravity torque;
I_i = moment of inertia of link I about centroidal axis parallel to z_i axis;
I_{zz1} = moment of inertia of crowd arm about centroidal axis parallel to z_1 axis;
I_{zz2} = moment of inertia of dipper about centroidal axis parallel to z_2 axis;
$\boldsymbol{k}_{zi}$ = unit vector on the z_i axis;
k_z = index for the type of cutting;
L_1 = length of crowd arm from pivotal point to the connection point between arm and dipper $(L_1=l_1)$;
L_2 = length between dipper tip and connect point of arm and dipper $(L_2=l_2)$;
m_i = mass of link i;
m_1 = mass of crowd arm;
m_2 = mass of dipper;
${}^1N_1$ = torque at the center of the crowd arm;
${}^2N_2$ = torque at the center of the dipper;
${}^0P_1$ = location vector for the rotation point of the crowd arm;
${}^1P_{c_1}$ = location vector for the center of the mass of the crowd arm;
${}^1_0R$ = transformation matrix from base frame to the crowd arm based coordinate;
r_i = length of line segment between O_{i-1} and O_i, $i=1,2,3$;
s = cutting edge index;
${}^1\dot{v}_{c_1}$ = linear acceleration at the center of the crowd arm;
${}^2\dot{v}_{c_2}$ = linear acceleration at the center of the dipper;
w = cutting tool width;
β = angle the rupture failure plane makes with the horizontal;
Γ_{ij} = (i,j) element of control matrix $\Gamma(\theta)$;
Θ = vector of generalized variables;
θ_b = angle between dipper bottom and X_4 axis;
θ_{dg} = angle between dipper edge and horizontal line (digging angle);
θ_i = angle between r_i and x axis of a local coordinate $(i=5,6,7,8,9,10,11)$;
θ_i, $\dot{\theta}_i$, $\ddot{\theta}_i$ = angular, velocity and acceleration of joint $i(i=1,2,3)$, respectively;
$\dot{\theta}_1$ = rotation angular velocity of the crowd arm based coordinate relative to the base frame;
θ_1, $\dot{\theta}_1$, $\ddot{\theta}_1$ = angular, velocity and acceleration of crowd arm, respectively;
${}^0\omega_0$ = angular velocity of the shovel base;
${}^0\dot{\omega}_0$ = angular acceleration of the shovel base;
${}^1\omega_1$ = angular velocity at the center of the crowd arm;
${}^1\dot{\omega}_1$ = angular acceleration at the center of the crowd arm;
${}^2\omega_2$ = angular velocity at the center of the dipper; and
${}^2\dot{\omega}_2$ = angular acceleration at the center of the dipper.

Appendix. Cable Shovel Dynamic Equations

The following equations describe the cable shovel kinematics and dynamic models in a typical surface mining operating environment. The base of the shovel is fixed, and hence it does not rotate during operation, resulting in

$$ {}^0\omega_0 = 0, \quad {}^0\dot{\omega}_0 = 0 \tag{2} $$

As an example, the outward iteration for crowd arm is demonstrated. This procedure includes the calculation of the angular velocity, angular acceleration, and the linear acceleration at the center of the crowd arm, respectively, in

$$ {}^1\omega_1 = {}^1_0R\,{}^0\omega_0 + \dot{\theta}_1\,{}^1\hat{Z}_1 = \begin{pmatrix} c_1 & s_1 & 0 \\ -s_1 & c_1 & 0 \\ 0 & 0 & 1 \end{pmatrix}\begin{pmatrix} 0 \\ 0 \\ 0 \end{pmatrix} + \begin{pmatrix} 0 \\ 0 \\ \dot{\theta}_1 \end{pmatrix} = \begin{pmatrix} 0 \\ 0 \\ \dot{\theta}_1 \end{pmatrix} \tag{3} $$

$$ {}^1\dot{\omega}_1 = {}^1_0R\,{}^0\omega_0 \times \dot{\theta}_1\,{}^1\hat{Z}_1 + {}^1_0R\,{}^0\dot{\omega}_0 + \ddot{\theta}_1\,{}^1\hat{Z}_1 = \begin{pmatrix} c_1 & s_1 & 0 \\ -s_1 & c_1 & 0 \\ 0 & 0 & 1 \end{pmatrix}\begin{pmatrix} 0 \\ 0 \\ 0 \end{pmatrix} \times \begin{pmatrix} 0 \\ 0 \\ \dot{\theta}_1 \end{pmatrix} + \begin{pmatrix} c_1 & s_1 & 0 \\ -s_1 & c_1 & 0 \\ 0 & 0 & 1 \end{pmatrix}\begin{pmatrix} 0 \\ 0 \\ 0 \end{pmatrix} + \begin{pmatrix} 0 \\ 0 \\ \ddot{\theta}_1 \end{pmatrix} = \begin{pmatrix} 0 \\ 0 \\ \ddot{\theta}_1 \end{pmatrix} \tag{4} $$

$$
\begin{aligned}
{}^1\dot{v}_1 &= {}^1_0R({}^0\dot{\omega}_0 \times {}^0P_1 + {}^0\omega_0 \times ({}^0\omega_0 \times {}^0P_1) + {}^0\dot{v}_0) + 2{}^1\omega_1 \times \dot{d}_1{}^1\hat{Z}_1 \\
&\quad + \ddot{d}_1{}^1\hat{Z}_1 \\
&= \begin{pmatrix} c_1 & s_1 & 0 \\ -s_1 & c_1 & 0 \\ 0 & 0 & 1 \end{pmatrix}\left\{\begin{pmatrix} 0 \\ 0 \\ 0 \end{pmatrix} \times \begin{pmatrix} 0 \\ 0 \\ 0 \end{pmatrix}\right\} + \begin{pmatrix} c_1 & s_1 & 0 \\ -s_1 & c_1 & 0 \\ 0 & 0 & 1 \end{pmatrix} \\
&\quad \times \left\{\begin{pmatrix} 0 \\ 0 \\ 0 \end{pmatrix} \times \left(\begin{pmatrix} 0 \\ 0 \\ 0 \end{pmatrix} \times \begin{pmatrix} 0 \\ 0 \\ 0 \end{pmatrix}\right) + \begin{pmatrix} 0 \\ g \\ 0 \end{pmatrix}\right\} + 2\begin{pmatrix} 0 \\ 0 \\ \dot{\theta}_1 \end{pmatrix} \times \begin{pmatrix} \dot{d}_1 \\ 0 \\ 0 \end{pmatrix} \\
&\quad + \begin{pmatrix} \ddot{d}_1 \\ 0 \\ 0 \end{pmatrix} = \begin{pmatrix} gs_1 + \ddot{d}_1 \\ gc_1 + 2\dot{d}_1\dot{\theta}_1 \\ 0 \end{pmatrix} \qquad (5)
\end{aligned}
$$

$$
\begin{aligned}
{}^1\dot{v}_{c_1} &= {}^1\dot{\omega}_1 \times {}^1P_{c_1} + {}^1\omega_1 \times ({}^1\omega_1 \times {}^1P_{c_1}) + {}^1\dot{v}_1 \\
&= \begin{pmatrix} -d_1\dot{\theta}_1^2 + \ddot{d}_1 + gs_1 \\ d_1\ddot{\theta}_1 + 2\dot{d}_1\dot{\theta}_1 + gc_1 \\ 0 \end{pmatrix} \qquad (6)
\end{aligned}
$$

It also involves the calculation of the torque and the inertial force at the center of the crowd arm, respectively, in

$$
\begin{aligned}
{}^1N_1 &= {}^{c_1}I_1{}^1\dot{\omega}_1 + {}^1\omega_1 \times {}^{c_1}I_1{}^1\omega_1 = \begin{pmatrix} 0 & 0 & 0 \\ 0 & 0 & 0 \\ 0 & 0 & I_{zz1} \end{pmatrix}\begin{pmatrix} 0 \\ 0 \\ \ddot{\theta}_1 \end{pmatrix} + \begin{pmatrix} 0 \\ 0 \\ \dot{\theta}_1 \end{pmatrix} \\
&\quad \times \left(\begin{pmatrix} 0 & 0 & 0 \\ 0 & 0 & 0 \\ 0 & 0 & I_{zz1} \end{pmatrix}\begin{pmatrix} 0 \\ 0 \\ \dot{\theta}_1 \end{pmatrix}\right) = \begin{pmatrix} 0 \\ 0 \\ I_{zz1}\ddot{\theta}_1 \end{pmatrix} \qquad (7)
\end{aligned}
$$

$$
{}^1F_1 = m_1{}^1\dot{v}_{c_1} = \begin{pmatrix} -m_1d_1\dot{\theta}_1^2 + m_1\ddot{d}_1 + m_1gs_2 \\ m_1d_1\ddot{\theta}_1 + 2m_1\dot{d}_1\dot{\theta}_1 + m_1gc_1 \\ 0 \end{pmatrix} \qquad (8)
$$

The angular velocity at the center of the crowd arm is necessary for estimating the Coriolis and centripetal effects of the crowd arm and dipper assembly. Using the gravity effect (${}^0\dot{v}_0 = g\hat{z}_0$), Eq. (5) can be reformulated as Eq. (6). The linear acceleration at the center of the crowd arm is used to calculate the inertial force of the crowd arm and dipper assembly. Euler's equation is used to calculate the torque at the mass center of the crowd arm, as illustrated in Eq. (7). Newton's equation is applied here to calculate the inertial force at the mass center of the crowd arm in Eq. (8).

The same procedure can be applied to the dipper to calculate its angular velocity, angular acceleration, linear acceleration, the torque at the center of the dipper, and the inertial force at the center of the dipper, as illustrated, respectively, in

$$
{}^2\omega_2 = {}^2_1R{}^1\omega_1 + \dot{\theta}_2{}^2\hat{Z}_2 = \begin{pmatrix} 1 & 0 & 0 \\ 0 & 1 & 0 \\ 0 & 0 & 1 \end{pmatrix}\begin{pmatrix} 0 \\ 0 \\ \theta_1 \end{pmatrix} + \begin{pmatrix} 0 \\ 0 \\ 0 \end{pmatrix} = \begin{pmatrix} 0 \\ 0 \\ \dot{\theta}_1 \end{pmatrix} \qquad (9)
$$

$$
\begin{aligned}
{}^2\dot{\omega}_2 &= {}^2_1R{}^1\omega_1 \times \dot{\theta}_2{}^2\hat{Z}_2 + {}^2_1R{}^1\dot{\omega}_1 + \ddot{\theta}_2{}^2\hat{Z}_2 \\
&= \begin{pmatrix} 1 & 0 & 0 \\ 0 & 1 & 0 \\ 0 & 0 & 1 \end{pmatrix}\begin{pmatrix} 0 \\ 0 \\ \dot{\theta}_1 \end{pmatrix} \times \begin{pmatrix} 0 \\ 0 \\ 0 \end{pmatrix} + \begin{pmatrix} 1 & 0 & 0 \\ 0 & 1 & 0 \\ 0 & 0 & 1 \end{pmatrix}\begin{pmatrix} 0 \\ 0 \\ \ddot{\theta}_1 \end{pmatrix} \\
&\quad + \begin{pmatrix} 0 \\ 0 \\ 0 \end{pmatrix} = \begin{pmatrix} 0 \\ 0 \\ \ddot{\theta}_1 \end{pmatrix} \qquad (10)
\end{aligned}
$$

$$
\begin{aligned}
{}^2\dot{v}_2 &= {}^2_1R({}^1\dot{\omega}_1 \times {}^1P_2 + {}^1\omega_1 \times ({}^1\omega_1 \times {}^1P_2) + {}^1\dot{v}_1) \\
&\quad + 2{}^2\omega_2 \times \dot{d}_2{}^2\hat{Z}_2 + \ddot{d}_2{}^2\hat{Z}_2 = \begin{pmatrix} -l_1\dot{\theta}_1^2 + \ddot{d}_1 + gs_1 \\ l_1\ddot{\theta}_1 + 2\dot{d}_1\dot{\theta}_1 + gc_1 \\ 0 \end{pmatrix} \qquad (11)
\end{aligned}
$$

$$
\begin{aligned}
{}^2\dot{v}_{c_2} &= {}^2\dot{\omega}_2 \times {}^2P_{c_2} + {}^2\omega_2 \times ({}^2\omega_2 \times {}^2P_{c_2}) + {}^2\dot{v}_2 \\
&= \begin{pmatrix} -(l_1 + d_2)\dot{\theta}_1^2 + \ddot{d}_1 + gs_1 \\ (l_1 + d_2)\ddot{\theta}_1 + 2\dot{d}_1\dot{\theta}_1 + gc_1 \\ 0 \end{pmatrix} \qquad (12)
\end{aligned}
$$

$$
\begin{aligned}
{}^2N_2 &= {}^{c_2}I_2{}^2\dot{\omega}_2 + {}^2\omega_2 \times {}^{c_2}I_2{}^2\omega_2 \\
&= \begin{pmatrix} 0 & 0 & 0 \\ 0 & 0 & 0 \\ 0 & 0 & I_{zz2} \end{pmatrix}\begin{pmatrix} 0 \\ 0 \\ \ddot{\theta}_1 \end{pmatrix} + \begin{pmatrix} 0 \\ 0 \\ \dot{\theta}_1 \end{pmatrix} \times \left(\begin{pmatrix} 0 & 0 & 0 \\ 0 & 0 & 0 \\ 0 & 0 & I_{zz4} \end{pmatrix}\right. \\
&\quad \left.\times \begin{pmatrix} 0 \\ 0 \\ \dot{\theta}_1 \end{pmatrix}\right) = \begin{pmatrix} 0 \\ 0 \\ I_{zz2}\ddot{\theta}_1 \end{pmatrix} \qquad (13)
\end{aligned}
$$

$$
{}^2F_2 = m_2{}^2\dot{v}_{c_2} = \begin{pmatrix} -m_2(l_1 + d_2)\dot{\theta}_1^2 + m_2\ddot{d}_1 + m_2gs_1 \\ m_2(l_1 + d_2)\ddot{\theta}_1 + 2m_2\dot{d}_1\dot{\theta}_1 + m_2gc_1 \\ 0 \end{pmatrix} \qquad (14)
$$

Having computed the forces and torques acting on the crowd arm and the dipper, it now remains to calculate the joint torques which will result in these net forces and torques being applied to the crowd arm and the dipper. This is achieved by writing force and moment balance equations based on free body diagrams of the crowd arm and the dipper. The inward iteration for the dipper is first calculated as

$$
\begin{aligned}
{}^2f_2 &= {}^3_2R^3f_3 + {}^2F_2 \\
&= \begin{pmatrix} -m_2(l_1 + d_2)\dot{\theta}_1^2 + m_2\ddot{d}_1 + f_{31}c_3 - f_{32}s_3 + m_2gs_1 \\ m_2(l_1 + d_2)\ddot{\theta}_1 + 2m_2\dot{d}_1\dot{\theta}_1 + f_{31}s_3 + f_{32}c_3 + m_2gc_1 \\ 0 \end{pmatrix} \qquad (15)
\end{aligned}
$$

Eq. (15) is the force balance equation for the dipper. The torque balance equation for the dipper is given by

$$ {}^2n_2 = {}^2N_2 + {}^2_3R^3n_3 + {}^2P_{c_2} \times {}^2F_2 + {}^2P_3 \times {}^2_3R^3f_3 = \begin{pmatrix} 0 \\ 0 \\ I_{zz2}\ddot{\theta}_1 + m_2(l_1 + d_2)d_2\ddot{\theta}_1 + 2m_2d_2\dot{d}_1\dot{\theta}_1 + m_2gd_2c_1 + f_{31}l_2s_3 + f_{32}l_2c_3 \end{pmatrix} \tag{16} $$

Following the same procedure, the inward iteration for crowd arm is given by

$$ {}^1f_1 = {}^2_1R^2f_2 + {}^1F_1 = \begin{pmatrix} -(m_1d_1 + m_2(l_1 + d_2))\dot{\theta}_1^2 + (m_1 + m_2)\ddot{d}_1 + f_{31}c_3 - f_{32}s_3 + (m_1 + m_2)gs_1 \\ (m_1d_1 + m_2(l_1 + d_2))\ddot{\theta}_1 + 2(m_1 + m_2)\dot{d}_1\dot{\theta}_1 + f_{31}s_3 + f_{32}c_3 + (m_1 + m_2)gc_1 \\ 0 \end{pmatrix} \tag{17} $$

$$ \begin{aligned} {}^1n_1 &= {}^1N_1 + {}^1_2R^2n_2 + {}^1P_{c_1} \times {}^1F_1 + {}^1P_2 \times {}^1_2R^2f_2 \\ &= \begin{pmatrix} 0 \\ 0 \\ (I_{zz1} + I_{zz2})\ddot{\theta}_1 + m_2(l_1 + d_2)d_2\ddot{\theta}_1 + 2m_2d_2\dot{d}_1\dot{\theta}_1 \end{pmatrix} \\ &\quad + \begin{pmatrix} 0 \\ 0 \\ m_2gd_2c_1 + f_{31}l_2s_3 + f_{32}l_2c_3 \end{pmatrix} \\ &\quad + \begin{pmatrix} 0 \\ 0 \\ m_1d_1^2\ddot{\theta}_1 + 2m_1d_1\dot{d}_1\dot{\theta}_1 + m_1gd_1c_1 + m_2(l_1 + d_2)l_1\ddot{\theta}_1 \end{pmatrix} \\ &\quad + \begin{pmatrix} 0 \\ 0 \\ 2m_2l_1\dot{d}_1\dot{\theta}_1 + f_{31}l_1s_3 + f_{32}l_1c_3 + m_2gl_1c_1 \end{pmatrix} \end{aligned} \tag{18} $$

Eqs. (17) and (18) are the respective force and moment balance equations for the crowd arm. Finally, the equations for the joint force and torque are obtained in

$$ \begin{aligned} F_1 &= (m_1 + m_2)\ddot{d}_1 - m_1d_1\dot{\theta}_1^2 - m_2(l_1 + d_2)\dot{\theta}_1^2 \\ &\quad + f_{31}c_3 - f_{32}s_3 + (m_1 + m_2)gs_1 \end{aligned} \tag{19} $$

$$ \begin{aligned} \tau_1 &= (I_{zz1} + I_{zz2})\ddot{\theta}_1 + (m_1d_1^2 + m_2(l_1 + d_2)^2)\ddot{\theta}_1 \\ &\quad + 2(m_1d_1 + m_2(l_1 + d_2))\dot{d}_1\dot{\theta}_1 + f_{31}(l_1 + l_2)s_3 + f_{32}(l_1 + l_2)c_3 \\ &\quad + (m_1d_1 + m_2(l_1 + d_2))gc_1 \end{aligned} \tag{20} $$

For cable shovels, Θ is equal to $\{d_1\ \theta_1\}^T$. From Eqs. (19) and (20), $D(\Theta)$, $C(\Theta, \dot{\Theta})$, $G(\Theta)$, and $F_{\text{load}}(F_t, F_n)$ can be determined, respectively, as

$$ D(\Theta) = \begin{bmatrix} m_1 + m_2 & 0 \\ 0 & I_{zz1} + I_{zz2} + m_1d_1^2 + m_2(l_1 + d_2)^2 \end{bmatrix} \tag{21} $$

$$ C(\Theta, \dot{\Theta}) = \begin{bmatrix} 0 & (m_1d_1 + m_2(l_1 + d_2))\dot{\theta}_1 \\ 2(m_1d_1 + m_2(l_1 + d_2))\dot{\theta}_1 & 0 \end{bmatrix} \tag{22} $$

$$ G(\Theta) = \begin{bmatrix} (m_1 + m_2)gs_1 \\ (m_1d_1 + m_2(l_1 + d_2))gc_1 \end{bmatrix} \tag{23} $$

$$ F_{\text{load}}(F_t, F_n) = \begin{bmatrix} f_{31}c_3 - f_{32}s_3 \\ f_{31}(l_1 + l_2)s_3 + f_{32}(l_1 + l_2)c_3 \end{bmatrix} \tag{24} $$

The dipper-environment geometrical relationships are illustrated in Fig. 4. Therefore, Eq. (24) can be written as

$$ F_{\text{load}}(F_t, F_n) = \begin{bmatrix} 1 & 0 & 0 \\ 1 & 1 & 0 \\ 1 & 1 & 1 \end{bmatrix} \times \begin{Bmatrix} r_4(-F_t \sin\theta_b - F_n \cos\theta_b) \\ r_3(-F_t \sin(\theta_{dg} - \theta_2 - \theta_3) - F_n \cos(\theta_{dg} - \theta_2 - \theta_3)) \\ r_2(-F_t \sin(\theta_{dg} - \theta_2) - F_n \cos(\theta_{dg} - \theta_2)) \end{Bmatrix} \tag{25} $$

From Figs. 4 and 9, it is noted that arm crowd and arm rotation have different trends. f_{31} and f_{32} can be related to F_r as in

$$ \begin{aligned} f_{31} &= -F_r \cos(\theta_1 - \theta_{dg} + 0.1) \\ f_{32} &= -F_r \sin(\theta_1 - \theta_{dg} + 0.1) \end{aligned} \tag{26} $$

Zelenin et al. (1985) provided a basis for estimating the resistive force, F_r, as shown in the following equation and Fig. 9:

$$ F_r = 10C_0d^{1.35}(1 + 2.6w)(1 + 0.0075\beta)(1 + 0.03s)e_zk_z \tag{27} $$

References

Araya, H., Kakuzen, M., Kimura, N., and Hayashi, N. (1988). "Automatic control system for hydraulic shovels." *Proc., U.S.–Japan Symp. on Flexible Automation—Crossing Bridges: Advances in Flexible Automation and Robotics*, Minneapolis.

Awuah-Offei, K. (2005). "Dynamic modeling of cable shovel formation interactions for efficient oil sands excavation." Ph.D. dissertation, Univ. of Missouri-Rolla, Rolla, Mo.

Craig, J. J. (1986). *Introduction to robotics: Mechanics and control*, Addison-Wesley, Reading, Mass.

Daneshmend, L., Hendricks, C., Wu, S., and Scoble, M. (1993). "Design of a mining shovel simulator." *Innovative mine design for the 21st Century*, Baiden and Archibald, eds., Kingston, Canada, 551–561.

Frimpong, S., and Hu, Y. (2004). "Parametric simulation of shovel-oil sands interactions during excavation." *Int. J. Surf. Mining, Reclamation & Environ.*, in press.

Frimpong, S., Hu, Y., and Szymanski, J. (2003). "Intelligent cable shovel excavation in surface mining." *SME Conf. and Annual General Meeting*, Cincinnati.

Frimpong, S., Szymanski, J., Pedrycz, W., and Gao, Y. (2001). "Intelli-

gent shovel excavation in varying oil sands formation and bitumen content." *Proposal, submitted to COURSE*, Univ. of Alberta, Edmonton, Alta., Canada.

Hendricks, C., Daneshmend, L., Wu, S., and Scoble, M. (1993). "Design of a simulator for productivity analysis of electric mining shovels." *Proc., 2nd Int. Symp. on Mine Mechanization and Automation*, Lulå, Sweden, 329–336.

Koivo, A. J. (1994). "Kinematics of excavators (backhoes) for transferring surface material." *J. Aerosp. Eng.*, 7(1), 17–32.

Koivo, A. J., Thoma, M., Kocaoglan, E., and Andrade-Cetto, J. (1996). "Modeling and control of excavator dynamics during digging operation." *J. Aerosp. Eng.*, 9(1), 10–18.

P&H Mining. (2003). *Peak performance practices: Excavator selection for high production, low-cost operations*, Harnischfeger Corporation, Milwaukee.

Vaha, P. K., and Shibniewski, M. J. (1993). "Dynamic model of excavator." *J. Aerosp. Eng.*, 6(2), 148–166.

Zelenin, A. N., Balovnev, V. I., and Kerov, I. P. (1985). *Machines for moving the Earth*, Amerind, New Delhi, India.